Functional characterization and proteomic analysis of the nucleocapsid protein of porcine deltacoronavirus

Sunhee Lee, Changhee Lee *

Animal Virology Laboratory, School of Life Sciences, BK21 plus KNU Creative BioResearch Group, Kyungpook National University, Daegu 702-701, South Korea

ABSTRACT

Porcine deltacoronavirus (PDCoV) is a newly discovered enterotropic swine coronavirus that causes enteritis and diarrhea in piglets. Like other coronaviruses, PDCoV commonly contains 4 major structural proteins: spike (S), envelope (E), membrane (M), and nucleocapsid (N) proteins. Among these, the N protein is known to be the most abundant and multifunctional viral component. Therefore, as the first step toward understanding the biology of PDCoV, the present study investigated functional characteristics and expression dynamics of host proteins in a stable porcine cell line constitutively expressing the PDCoV N protein. Similar to N proteins of other coronaviruses, the PDCoV N protein was found to interact with itself to form non-covalently linked oligomers and was mainly localized to the nucleolus. We then assessed alterations in production levels of proteins in the N-expressing PK (PK-PDCoV-N) cells at different time points by means of proteomic analysis. According to the results of high-resolution two-dimensional gel electrophoresis, a total of 43 protein spots were initially found to be differentially expressed in PK-PDCoV-N cells in comparison with control PK cells. Of these spots, 10 protein spots showed a statistically significant alteration, including 8 up-regulated and 2 down-regulated protein spots and were picked for subsequent protein identification by peptide mass fingerprinting following matrix-assisted laser desorption/ionization time-of-flight mass spectrometry. The affected cellular proteins that we identified in this study were classified into the functional groups involved in various cellular processes such as cell division, metabolism, the stress response, protein biosynthesis and transport, cytoskeleton networks and cell communication. Notably, two members of the heat shock protein 70 family were found to be up-regulated in PK-PDCoV-N cells. These proteomic data will provide insights into the specific cellular response to the N protein during PDCoV infection.

© 2015 Elsevier B.V. All rights reserved.

1. Introduction

Porcine deltacoronavirus (PDCoV) is an emerging viral pathogen that was first reported in 2012 in Hong Kong, China (Woo et al., 2012). In February 2014, the detection of PDCoV was first announced in Ohio, United States, in conjunction with outbreaks of diarrhea without other etiologic agents. Since its emergence, this novel coronavirus has been detected in 17 US states, and almost 80% of the tested samples corresponded to cases of coinfection of PDCoV with other enteric viral pathogens such as a rotavirus or porcine epidemic diarrhea virus (Li et al., 2014; Marthaler et al.,

2014a,b; Wang et al., 2014). Furthermore, recent independent studies demonstrated that PDCoV can cause severe enteric lesions and clinical diarrhea in the absence of other pathogens in neonatal and gnotobiotic pigs (Jung et al., 2015). Shortly thereafter, PDCoV was identified in Korea in 2 fecal samples independently collected in April and June 2014, and each of which were positive for a rotavirus and negative for other enteric viruses (Lee and Lee, 2014). Genetic and phylogenetic analyses showed that these Korean strains are more closely related to the US strains than to the Hong Kong HKU15 strains (Lee and Lee, 2014).

PDCoV is a large, enveloped virus possessing a single-stranded, positive-sense RNA genome of approximately 25.4 kb with a 5′ cap and a 3′ polyadenylated tail, belonging to the genus *Deltacoronavirus* within the family *Coronaviridae* of the order *Nidovirales* (de Groot et al., 2011; Woo et al., 2012). The PDCoV genome contains six common coronaviral genes in the following conserved order: 5′ untranslated region (UTR)-ORF1a-ORF-1b-S-E-M-N-3′

UTR. ORF1a/b encompasses two-thirds of the genome encoding 2 overlapping viral replicase polyproteins, 1a and 1ab, which are then proteolytically processed into mature nonstructural proteins. As in other coronaviruses, production of polyproteins 1a and 1ab requires a −1 ribosomal frameshift during translation of the genomic RNA. The last third of the genome encodes the 4 structural proteins, spike (S), envelope (E), membrane (M), and nucleocapsid (N), as well as two accessory genes, nonstructural gene 6 (NS6) and NS7 gene, between M and N, and within N, respectively (Lai et al., 2007; Lee and Lee, 2014; Li et al., 2014; Marthaler et al., 2014a; Woo et al., 2012).

Among the structural proteins of coronaviruses, the N protein is abundantly produced in infected cells and has multiple functions in viral replication and pathogenesis (McBride et al., 2014). As the sole structural component of the viral capsid, the N protein of coronaviruses interacts with the nucleic acid and itself for self-association to protect the viral genome from extracellular agents, serving as the critical basis for ribonucleoprotein (RNP) complexes during virus assembly (McBride et al., 2014). The entire life cycle of coronaviruses takes place in the cytoplasm of infected cells, and accordingly, the N protein is distributed mainly in the cytoplasmic compartments. In addition to their cytoplasmic localization, coronaviral N proteins are commonly localized to the nucleolus, suggesting their non-structural functions in ensuring successful virus infection (Hiscox et al., 2001; McBride et al., 2014). Although a variety of studies have confirmed that N possesses multifunctional significance in coronavirology (McBride et al., 2014), detailed characteristics of this protein and its role in the replication of PDCoV remain unknown.

In the present study, alterations in cellular gene expression that are caused by the N protein were evaluated as a first step toward understanding the biological role of the N protein in PDCoV replication. To accomplish this task, stable porcine-origin cell lines constitutively expressing the PDCoV N protein were generated and characterized in this study. Changes in expression patterns of various cellular proteins in the N protein-expressing porcine cells in comparison with control cells were examined by proteomic analysis at different time points. Our proteomic data are expected to provide novel information for better knowledge of the properties and functions of the N protein during PDCoV infection.

2. Materials and methods

2.1. Cells and antibodies

HEK-293T cells (CRL-1573) were purchased from the American Type Culture Collection (ATCC, Manassas, VA) and cultured in Dulbecco's modified Eagle medium (DMEM) with high glucose (Invitrogen, Carlsbad, CA) with 10% fetal bovine serum (FBS; Invitrogen) and antibiotic–antimycotic solutions (100×; Invitrogen). PK-15 cells were grown in RPMI 1640 medium (Invitrogen) supplemented with 10% FBS and antibiotic–antimycotic solutions (100×). The cells were maintained at 37 °C in an atmosphere of humidified air containing 5% CO_2. PAM-pCD163-N cells that stably express the N protein of porcine reproductive and respiratory syndrome virus (PRRSV; Sagong and Lee, 2010) were cultured in RPMI 1640 medium (Invitrogen) supplemented with 10% FBS, antibiotic–antimycotic solutions (100×), 10 mM HEPES (Invitrogen), 1 mM sodium pyruvate (Invitrogen), and nonessential amino acids (100×; Invitrogen) in the presence of 50 μg/ml Zeocin (Invitrogen) and 200 μg/ml G418 (Invitrogen). The anti-PRRSV nucleocapsid (N) monoclonal antibody (MAb) and anti-myc MAb were purchased from MEDIAN Diagnostics (Chuncheon, South Korea) and Invitrogen, respectively. Antibodies to the 6× histidine tag, glucose-regulated protein 78 (GRP78), heat shock cognate 70-kDa protein (HSC70), β-actin, α-tubulin, and Sp1 were purchased from Santa Cruz Biotechnology (Santa Cruz, CA).

2.2. Construction of the PDCoV N plasmid

DNA manipulation and cloning were performed according to standard procedures (Sambrook and Russell, 2001). The Escherichia coli strain DH5α (RBC Bioscience, Taiwan) was used as the host for general cloning. The full-length N gene was amplified from the PDCoV KNU14-04 strain (Lee and Lee, 2014) with the following primer pair: KNU14-04-N-Fwd (5′-GCCGGTCGACATGGCTGCACCAGTAG-3′) and KNU14-04-N-Rev (5′-CGGCTCTAGACGCTGCTGATTCCTGC-3′), where underlines indicate the SalI and XbaI restriction enzyme sites, respectively. The PCR amplicon was initially inserted into the pBudCE4.1 vector (Invitrogen) that contains a myc epitope and 6 repetitive histidine codons, and the resulting plasmid pBud-PDCoV-N was verified by nucleotide sequencing. Because the PDCoV genome contains one accessory NS7 gene within the N gene in a different reading frame, the presence of NS7 could affect our functional studies of the PDCoV N protein. To prevent any such side effects, the translation initiation codon and the fifth codon of the NS7 ORF were modified to disrupt its expression by pBud-PDCoV-N. To accomplish this, overlapping PCR was conducted to simultaneously change the ATG start codon and the fifth codon of the NS7 gene to TTA and TAA at genomic nucleotide positions 24,096–24,098 and 24,108–24,110, respectively, using pBud-PDCoV-N as a template with the following primers for the T24097C/T24109A mutation: NS7-KO-Fwd (5′-GGCAAcGGAGTTCCGCTaAACTCCGCCATC-3′) and NS7-KO-Rev (5′-GATGGCGGAGTTtAGCGGAACTCCgTTGCC-3′), where lowercase letters indicate the mutated nucleotides. Both mutations were translationally silent with respect to the ORF encoding the N protein, and the resulting plasmid pBud-PDCoV-N$^{w/oNS7}$ was verified by nucleotide sequencing. A fragment of PDCoV N $^{w/oNS7}$ cDNA that was prepared from pBud-PDCoV-N was then subcloned into the pFB-Neo retroviral vector (Stratagene, La Jolla, CA) using the SalI and EcoRI restriction sites to construct the PDCoV N gene expression plasmid pFB-Neo-PDCoV-N-myc/His that produces recombinant N protein.

2.3. Generation of stable PK-15 cell lines expressing the PDCoV N protein

The retrovirus gene transfer system (Stratagene) was used to generate cell lines constitutively expressing the recombinant PDCoV N gene or an empty vector only as described elsewhere (Lee et al., 2010; Nam and Lee, 2010; Oh and Lee, 2012). Antibiotic-resistant continuous cell clones were analyzed by RT-PCR to determine the presence of the full-length N gene, and the positive clones (PK-PDCoV-N and PK-Neo) were amplified for subsequent experiments.

2.4. Immunofluorescence assay (IFA)

PK-PDCoV-N cells were grown on microscope coverslips placed in 6-well tissue culture plates. At 48 h post-seeding, the cells were fixed with 4% paraformaldehyde for 10 min at room temperature (RT) and permeabilized with 0.2% Triton X-100 in PBS at RT for 10 min. The cells were blocked using 1% bovine serum albumin (BSA) in PBS for 30 min at RT and then incubated with an anti-His tag or anti-myc antibody for 2 h. After washing 5 times in PBS, the cells were incubated for 1 h at RT with a goat anti-mouse secondary antibody conjugated with Alexa Fluor 488 (Molecular Probes, Carlsbad, CA). The cells were finally counterstained with 4′,6-diamidino-2-phenylindole (DAPI; Sigma, St. Louis, MO), and the cell staining was visualized by the fluorescence Leica DM IL LED microscope (Leica,

Wetzlar, Germany) or a Confocal Laser Scanning microscope (Carl Zeiss, Gattingen, Germany).

2.5. Fluorescence-activated cell sorting (FACS) analysis

The N expression in PK-PDCoV-N cells was analyzed by flow cytometry. The cells were trypsinized at 48 h post-seeding and centrifuged at $250 \times g$ (Hanil Centrifuge FLETA 5) for 5 min. The cell pellet was washed with cold washing buffer (1% BSA and 0.1% sodium azide in PBS), and 10^6 cells were resuspended in 1% formaldehyde solution in cold wash buffer for fixation at $4 \,^\circ$C in the dark for 30 min followed by centrifugation and incubation of the pellet in 0.2% Triton X-100 in PBS at $37 \,^\circ$C for 15 min for permeabilization. After centrifugation, the cell pellet was resuspended in a solution of the primary anti-His tag antibody or normal mouse IgG1 (Santa Cruz Biotechnology) and the mixture was incubated at $4 \,^\circ$C for 30 min. The cells were washed and allowed to react with an Alexa Fluor 488-conjugated anti-mouse IgG secondary antibody at $4 \,^\circ$C for 30 min in the dark. The stained cells were washed again and analyzed on the BD FACSAria III flow cytometer (BD Biosciences, Belford, MA).

2.6. Cell proliferation assay

The growth properties of cells expressing PDCoV N protein and control cells were determined by a 3-(4,5-dimethylthiazol-2-yl)-2,5-diphenyltetrazolium bromide (MTT) assay (Sigma) detecting cell viability as described previously (Kim and Lee, 2013). All MTT assays were performed in triplicate.

2.7. Cell fractionation and Western blot analysis

Whole cell lysates were prepared from PK-PDCoV-N cells grown at 5×10^5 cells/well in 6-well tissue culture plates at indicated time points using lysis buffer as described previously (Nam and Lee, 2010). For cell fractionation, PK-PDCoV-N cells were fractionated using the Nuclear/Cytosol Fractionation Kit (BioVision, Mountain View, CA) according to the manufacturer's manuals. The protein concentrations of the cell lysates were determined using the BCA protein assay (Pierce, Rockford, IL). The cell lysates were mixed with $4\times$ NuPAGE sample buffer (Invitrogen) and boiled at $70 \,^\circ$C for 10 min. Equal amounts of total protein were separated in a NuPAGE 4–12% Gradient Bis-Tris Gel (Invitrogen) under non-reducing or reducing conditions, and electrotransferred onto an Immobilon-P membrane (Millipore, Billerica, MA). The membranes were blocked with 3% powdered skim milk (BD Biosciences) in TBS (10 mM Tris–HCl [pH 8.0], 150 mM NaCl) with 0.05% Tween-20 (TBST) at $4 \,^\circ$C for 2 h and reacted with the primary antibody against the $6\times$ His-tag, GRP78, HSC70, or β-actin at $4 \,^\circ$C overnight. The blots were then incubated with a horseradish peroxidase (HRP)-labeled goat anti-mouse IgG or goat anti-rabbit IgG antibody (Santa Cruz Biotechnology) at the dilution of 1:2000 for 2 h at $4 \,^\circ$C. Finally, the proteins were visualized by enhanced chemiluminescence (ECL) Reagents (Amersham Biosciences, Piscataway, NJ) according to the instructions of the manufacturer. To analyze the expression kinetics of cellular proteins in PK-PDCoV-N cells, the band density of each protein was quantified relative to β-actin using densitometry with the Wright Cell Imaging Facility (WCIF) version of the ImageJ software package (http://www.uhnresearch.ca/facilities/wcif/imagej/).

2.8. Chemical cross-linking

A chemical cross-linking assay was performed as described previously (Lee and Yoo, 2006). Briefly, PK-PDCoV-N cells and PAM-pCD163-N cells were grown in a 6-well tissue culture plate for 48 h. For cross-linking studies, the cells were washed twice with cold PBS and then incubated at RT for 30 min with a 2 mM solution of a membrane permeable and thiol-cleavable cross-linker, 3,3′-dithiobis(succinimidyl propionate) (DSP; Pierce), dissolved in 10% dimethyl sulfoxide (v/v in PBS). The reaction was quenched with 50 mM Tris–HCl [pH 7.5] and incubated for an additional 15 min. The cells were lysed with lysis buffer, and the resultant cell lysates were then subjected to a Western blot assay as described above.

2.9. Preparation of protein samples for proteomic analysis

Pellets of cultured cells were washed twice with ice-cold PBS, placed in sample lysis solution consisting of 7 M urea, 2 M thiourea, 4% 3-[(3-cholamidopropyl) dimethyammonio]-1-propanesulfonate (CHAPS), 1% dithiothreitol (DTT), 2% pharmalyte (pH 3.5–10, Amersham Biosciences), and 1 mM benzamidine, and were then sonicated for 10 s using a Sonoplus device (Bandelin Electronic, Germany). The samples were subsequently incubated for 1 h at $4 \,^\circ$C. After centrifugation at $15,000 \times g$ for 1 h at $4 \,^\circ$C, insoluble cellular debris were discarded, and the supernatant was collected and stored at $-80 \,^\circ$C until use. The protein concentrations were measured by the Bradford assay as described previously (Bradford, 1976).

2.10. Two-dimensional gel electrophoresis (2DE) and image analysis

Protein samples were analyzed by 2DE using commercial IPG dry strips (pH 4–10, 24 cm; Genomine Inc., Pohang, South Korea) for the first-dimensional separation (isoelectric focusing; IEF) and sodium dodecyl sulfate-polyacrylamide gel electrophoresis (SDS-PAGE) for the second dimension. The IPG dry strips were loaded independently with 200 μg of each protein sample and rehydrated overnight in rehydration buffer (7 M urea, 2 M thiourea, 2% CHAPS, 1% DTT, and 1% pharmalyte). IEF was performed at $20 \,^\circ$C using a Multiphor II electrophoresis unit and an EPS 3500 XL power supply (Amersham Biosciences) with the following parameters: gradient increase from 150 to 3500 V for 3 h and 3500 V for a total of 96,000 V h. Following IEF separation, the IPG strips were incubated for 10 min at RT with gentle shaking in equilibration buffer (50 mM Tris–Cl pH 6.8, containing 6 M urea, 2% SDS, and 30% glycerol) containing 1% DTT and were subsequently incubated in the equilibration buffer containing 2.5% iodoacetamide under the same conditions. Each equilibrated strip was then inserted into 10–16% polyacrylamide gels (20 cm × 24 cm) and SDS-PAGE was run using a Hoefer DALT 2D system (Amersham Biosciences) at $20 \,^\circ$C for 1700 V h according to the manufacturer's instructions. The 2D gels were stained by the silver staining method as described previously with some modifications (Oakley et al., 1980). To compensate for the variability of 2DE, three independent experiments were conducted for further statistical analysis.

The stained gels were imaged using a high-resolution 2D gel CCD image analyzer, Dyversity (Syngene, Frederick, MD), and quantitative analysis of the digitized gel images was carried out using the PDQuest software (version 7.0, Bio-Rad, Hercules, CA) according to the protocols provided by the manufacturer. Data representing 3 independent 2DE experiments for each sample were statistically analyzed using Student's t-test, and p-values of less than 0.05 were considered to be statistically significant. The quantitative data from each protein spot were normalized based on the total valid spot intensity for each gel. Only protein spots that showed significant differential expression ($p < 0.05$) with a ± 2-fold consistent change in the expression level in comparison with the control sample were selected for mass spectrometry (MS) analysis.

2.11. Protein identification by peptide mass fingerprinting (PMF)

Each selected protein spot was excised manually from the silver-stained gels and was enzymatically digested in-gel as previously described (Shevchenko et al., 1996) and using modified porcine trypsin (Sequencing grade; Promega, Madison, WI). The gel pieces were washed with 50% acetonitrile (ACN), air-dried thoroughly at RT, and then rehydrated for 8–10 h at 37 °C with modified sequencing grade porcine trypsin (8–10 ng/µl). The proteolytic reaction was terminated by addition of 5 µl of 0.5% trifluoroacetic acid (TFA). The tryptic peptides were recovered by combining the aqueous phase from several extractions of gel pieces with 50% aqueous ACN. After concentration, the peptide mixture was desalted using C_{18} ZipTips (Millipore), and the peptides were eluted in 1–5 µl of 50% ACN. An aliquot of this solution was mixed with an equal volume of a saturated solution of α-cyano-4-hydroxycinnamic acid (CHCA; Sigma) in 50% ACN/0.1% TFA, and 1 µl of this mixture was immediately spotted onto the target plate. MALDI-TOF analysis was performed on a Microflex LRF 20 instrument (Bruker Daltonics, Billerica, MA) as described by Fernandez et al. (1998). The spectra were collected from 300 shots per spectrum over the m/z range 600–3000 and calibrated by two point internal calibration using trypsin auto-digestion peaks (m/z 842.5099, 2211.1046). The peak list was generated using Flex Analysis 3.0. We used the following threshold for peak-picking: 500 for minimum resolution of monoisotopic mass, 5 for S/N. The search program MASCOT from Matrix Science (http://www.matrixscience.com/) was used for protein identification by PMF. The following parameters were used for the database search: trypsin as the cleaving enzyme, a maximum of one missed cleavage, iodoacetamide (Cys) as a complete modification, oxidation (Met) as a partial modification, monoisotopic masses, and a mass tolerance of ±0.1 Da. The PMF acceptance criterion was probability scoring.

2.12. Quantitative real-time RT-PCR

Total RNA was extracted from the lysates of PK-PDCoV-N cells at 24 and 48 h post-seeding by the TRIzol Reagent (Invitrogen) and was treated with DNase I (TaKaRa, Otsu, Japan) according to the manufacturer's protocols. The concentrations of the extracted RNA were measured using a NanoVue spectrophotometer (GE Healthcare, Piscataway, NJ). Quantitative real-time RT-PCR was performed using a Thermal Cycler Dice Real Time System (TaKaRa) with gene-specific primer sets as described previously (Sagong and Lee, 2011). The primer sequences are available upon request. The RNA levels of cellular genes were normalized to porcine β-actin mRNA, and relative quantities (RQ) of mRNA accumulation were calculated using the $2^{-\Delta\Delta Ct}$ method (Livak and Schmittgen, 2001). To detect alterations of cellular mRNA levels in the presence of the PDCoV N protein, the relative fold change of each cellular gene was calculated in accordance with the comparison of PK-PDCoV-N and control PK-Neo cells.

2.13. Statistical analysis

We used the Student's *t*-test for all statistical analyses, and differences with *p*-values <0.05 were considered statistically significant.

3. Results

3.1. Generation and characterization of stable porcine-origin cell lines expressing the PDCoV N protein

A set of seven novel mammalian and avian coronaviruses was recently discovered, including one porcine coronavirus, PDCoV (Woo et al., 2012). PDCoV is the fifth coronavirus infecting pigs in addition to transmissible gastroenteritis virus, porcine respiratory virus, porcine hemagglutinating encephalomyelitis virus, and porcine epidemic diarrhea virus (PEDV). To date, interactions between this novel virus and the host have not been studied yet. Furthermore, alterations of cellular protein expression in response to PDCoV or each viral protein upon infection currently remain undetermined. In the current study, the PDCoV N protein was chosen in the current study for the proteomic analysis to evaluate specific host cellular responses, which is not only the most abundant viral component but also performs several biological functions in completing viral replication. For this purpose, sublines of PK-15 cells were established to stably express recombinant PDCoV N under the control of a retroviral long-terminal-repeat (LTR) promoter. Ten generated cell clones were initially collected and subjected to RT-PCR and Western blotting to confirm the N gene expression at mRNA and protein levels, respectively (data not shown). According to the results of the Western blot analysis, one PK-PDCoV-N cell clone that constitutively expressed the highest levels of N was selected for subsequent studies.

To characterize PK-PDCoV-N cells, we examined intracellular expression levels of N by IFA, FACS analysis and Western blotting. As shown in Fig. 1A, the specific cell staining was clearly evident when PK-PDCoV-N cells were reacted with the anti-His tag antibody, confirming the constant high expression level of the N protein. Furthermore, the majority of the cells consistently exhibited specific fluorescent signals, indicating a homogenous population of cells in terms of N expression (Fig. 1B). Time-course Western blot analysis revealed that the PK-PDCoV-N cells stably express and accumulate robust levels of a ~45 kDa recombinant N protein, larger than its predicted molecular weight of approximately 38 kDa possibly due to post-translational modifications and the presence of C-terminal *myc* and histidine tags (Fig. 1C). In addition, the overall growth kinetics of PDCoV N gene-expressing PK cells was found to be similar to that of the parental PK-Neo cells, indicating that the PDCoV N expression has no effect on cell proliferation (Fig. 1D).

Self-association of the N protein has been observed in many viruses, including coronaviruses, and is essential for assembly of the viral core constructing the basic architecture of viruses. Sequence analysis of the PDCoV N protein indicated that it is composed of 342 amino acids residues and contains no cysteine residues. As expected, no band corresponding to a disulfide-linked N dimer was detected by SDS-PAGE under non-reducing conditions (Fig. 2A, lane 4), indicating that the PDCoV N protein does not undergo cysteine-linked homodimerization. As a positive control, the PRRSV N protein in the N-expressing stable PAM cells was clearly demonstrated to form 35-kDa N-N dimers under the same conditions (Sagong and Lee, 2010; Fig. 2A, lane 2). The ability of N to form non-covalent dimers was further investigated in a chemical cross-linking experiment. As shown in Fig. 2B, the PRRSV N protein in PAM-pCD163-N cells formed a number of higher-order oligomers (lane 1) as reported previously (Wootton and Yoo, 2003). When the N protein in PK-PDCoV cells was subjected to cross-linking, numerous multimeric forms of the N protein were identified (lane 2), indicating that the N protein of PDCoV exists in the form of non-covalently linked oligomers that are used for assembly the viral capsid.

We next determined whether the recombinant N protein expressed in PK-PDCoV-N cells is subject to nucleolar localization that is known to be a common feature of coronaviral N proteins. The staining pattern in PK-PDCoV cells was found to be predominantly cytoplasmic and nucleolic; this pattern persisted for up to 60 h after seeding (Fig. 3A). Nearly all cells expressing PDCoV N showed distinct fluorescent signals in the nucleolus at 48 h post-seeding, and
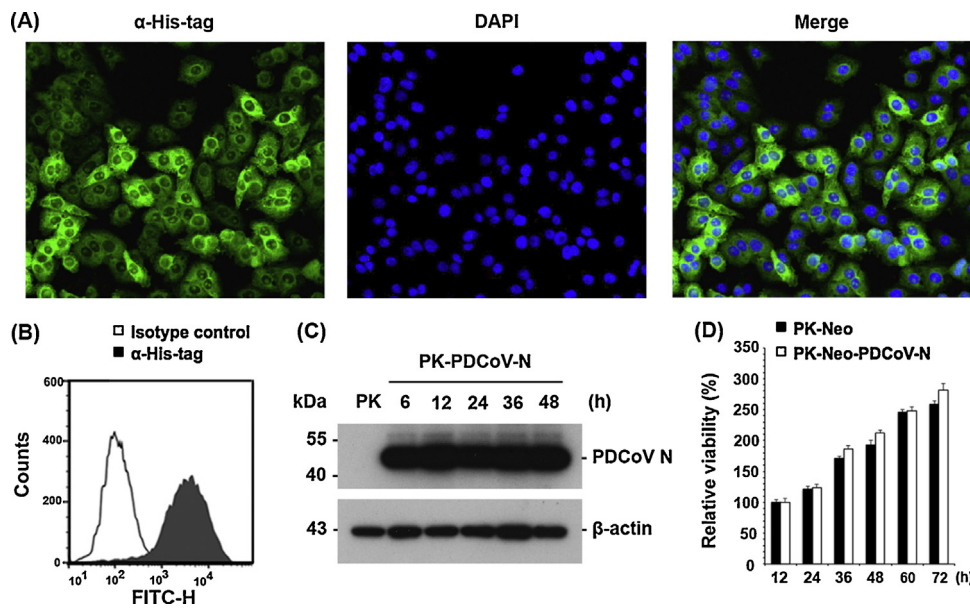
Fig. 1. Constitutive expression of the N protein in PK-PDCoV-N cells. (A) Immunofluorescence assay of the PDCoV N protein. PK-PDCoV-N cells grown in a 6-well tissue culture plate were fixed with 4% formaldehyde at indicated time points and incubated with the His tag-specific antibody followed by goat anti-mouse secondary antibody conjugated with Alexa green (upper panels). The cells were then counterstained with DAPI (middle panels) and examined using a fluorescent microscope at 400× magnification. (B) Intracellular expression of PDCoV N. One million cells were harvested at 48 h post-seeding and incubated with anti-His tag antibody (gray histogram) or an isotype control (white histogram) and analyzed by flow cytometry. (C) Immunoblot analysis of the N protein. PK-PDCoV-N cells were grown in a 6-well tissue culture plate at 4×10^5 cells/well for 6, 12, 24, 36, and 48 h. Cell lysates were prepared at the indicated time points and subjected to Western blot analysis with anti-His tag antibody to determine the expression level of the N protein (upper panel). The blot was also reacted with mouse MAb against β-actin to confirm equal protein loading (lower panel). (D). Growth kinetics of the stable PDCoV N protein expressing cells. Cell proliferation was measured at the indicated times by the MTT assay. Values are representative of the mean from three independent experiments and error bars denote standard deviations.
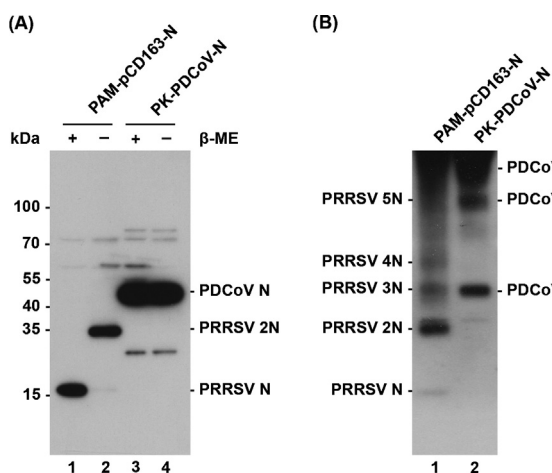
thereafter, the PDCoV N protein was localized mainly to the cytoplasm at 72 h post-seeding. The nucleolar localization of PDCoV N was confirmed by transient transfection of BHK-21 or ST cells with the plasmid pBud-PDCoV-N (Fig. 3B). The cell fractionation assay also revealed the presence of the N protein in both the cytoplasmic and nucleic fractions (Fig. 3C). These observations demonstrated that, like N proteins of other coronaviruses, PDCoV N protein is mostly distributed in the nucleolus along with the cytoplasm and has a conserved subcellular localization property.

Fig. 2. Homo-oligomerization of the PDCoV N protein. (A) Absence of the disulfide-linked N homodimers. Cell lysates were prepared from PAM-pCD163-N and PK-PDCoV-N cells grown for 48 h and subjected to Western blot analysis in the presence (lanes 1 and 3) or absence (lanes 2 and 4) of β-mercaptoethanol (βME). Monomers (N) and dimmers (2N) of the PRRSV N protein are indicated as positive controls. (B) N protein oligomerization by DSP cross-linking. Each cell line expressing PRRSV N (lane 1) or PDCoV N (lane 2) was independently cross-linked with 2 mM DSP for 30 min. Cell lysates were prepared and subjected to Western blot analysis under non-reducing conditions. Multimeric forms of N proteins of both viruses are shown.

3.2. 2DE analysis of porcine cells constitutively expressing the PDCoV N protein
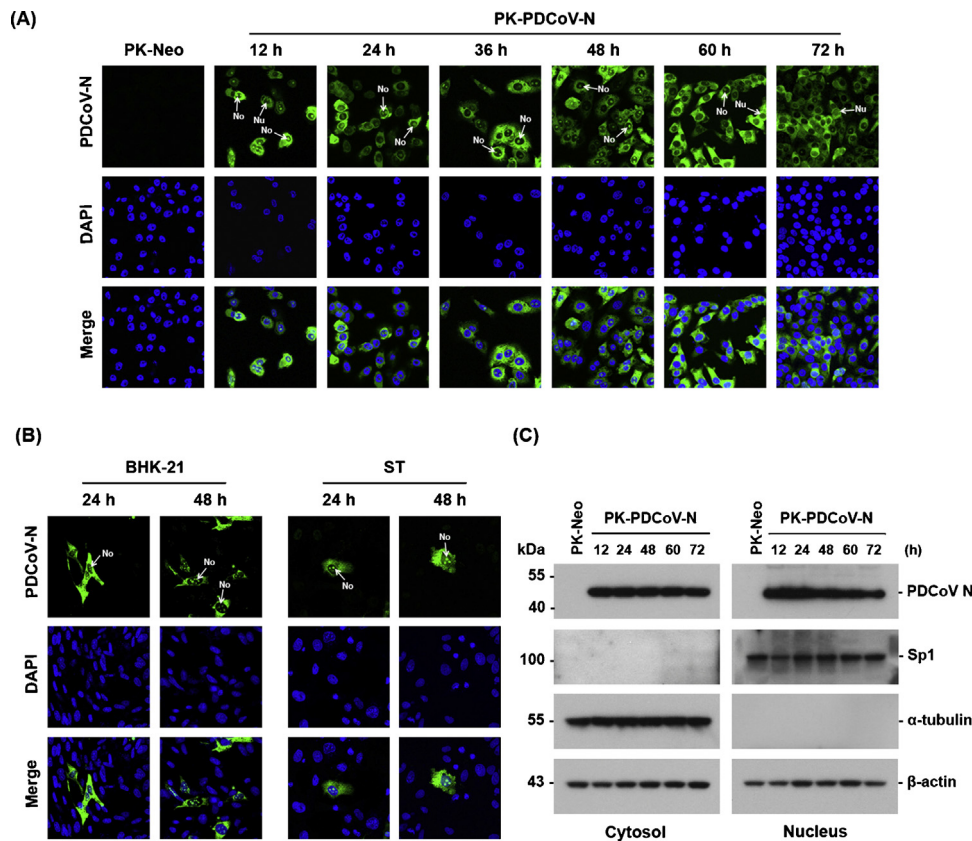
Cellular proteins in the parental PK-Neo cells and PK-PDCoV-N cells were extracted and subjected to 2DE analysis to compare the host protein expression profiles. To reduce the variability of gel electrophoresis, three independent 2DE analyses of cellular extracts from control or N gene-expressing PK cells were performed, and spot intensity data from triplicate gels were selected for statistical analysis. On average, 1090 ± 63 protein spots were resolved by 2DE within a pH gradient 4–10 and were visualized using silver staining; the molecular weights of the spots ranged from 10 to 200 kDa. These spots were used for the comparative analysis. Fig. 4A shows representative images of 2DE gels from control PK cells (upper panel) and N gene-expressing PK cells (middle and lower panels). A total of 43 protein spots were initially found to be differentially expressed in PK-PDCoV-N cells when compared with control PK-Neo cells. On the basis of the statistical comparison, only those spots that consistently showed alteration in expression levels between PK-PDCoV-N cells and the control cells were chosen for further protein identification.

3.3. Identification of the differentially expressed proteins

To identify the differentially expressed cellular protein spots in PK-PDCoV-N cells at different time points, 10 protein spots with a statistically significant alteration, including 8 up-regulated and 2 down-regulated protein spots (Fig. 4B), were selected and manually excised from the stained gels. Subsequently, the trypsin-digested spots were subjected to MALDI-TOF analysis. With combined PMF and database searching, identity of all 10 proteins was successfully determined. Information on all these proteins in PK-PDCoV-N cells, with their protein scores and sequence coverage, is summarized in Table 1. To better understand the implications of the cellular responses to the PDCoV N protein, we further

Fig. 3. Nucleolar localization of the PDCoV N protein expressed in PK-PDCoV-N cells. (A) Subcellular localization of N in cells stably expressing (A) and transiently expressing (B) PDCoV N. Cells were fixed at indicated time points post-seeding or post-transfection and incubated with anti-His or anti-*myc* tag MAb followed by Alexa green-conjugated goat anti-mouse secondary antibody. The cells were visualized using a fluorescent microscope at 400× magnification. Nucleus (Nu) and nucleolus (No) are indicated by arrows. (C) Nuclear and cytoplasmic fractionation of PK cells expressing PDCoV N. Each nuclear and cytosolic fraction was prepared from PK-PDCoV-N cells at indicated time points post-seeding and subjected to Western blot analysis with the antibody specific for His-tag (top panel), Sp1 as a nuclear protein marker (second panel), or α-tubulin as a cytosolic protein marker (third panel). All blots were also reacted with β-actin antibody to verify equal protein loading (bottom panel).

categorized the identified proteins by biological processes according to the Gene Ontology database as described previously (Zhang et al., 2009). These proteins showing altered expression were associated with various cellular functions including intracellular transport, metabolic processes, gene regulation, the stress response, protein synthesis, cytoskeleton networks, and cell division. Since changes in cellular protein expression may be attributed to alterations in the corresponding mRNA levels, transcriptional changes for all the identified proteins were tested by real-time RT-PCR to confirm the results of the proteomic analysis (Fig. 5).

We were able to detect mRNAs corresponding to nearly all proteins identified by proteomics, except for histone H4. Although the altered expression levels of the remaining 9 proteins were consistent with the real-time RT-PCR results, we observed only modest increase or reduction in mRNA levels. These results could be explained the case the correlation between mRNA and protein abundance could be insufficient to predict protein expression levels from quantitative mRNA data (Gygi et al., 1999), suggesting that the differences in protein levels might be due to post-translational modifications or protein stability rather than mRNA levels.

Table 1
List of differentially expressed cellular proteins in PDCoV N-expressing PK cells.

Spot no.	Protein name	Accession no.	MW (kDa)	pI	Protein score	Sequence coverage (%)	Function
Down-regulated proteins							
3006	Translocon-associated protein subunit delta isoform	gi|545887405	19.017	5.49	107	38	Protein transport to the ER
4009	Ferritin	gi|346421372	20.165	5.75	141	65	Metabolic process
Up-regulated proteins							
0019	Histone H4	gi|354480096	15.032	11.02	177	53	Gene regulation
1627	78 kDa glucose-regulated protein	gi|466006301	72.449	5.06	163	35	Stress response
1636	Heat shock 70 kDa protein 8	gi|345441750	71.050	5.37	281	36	Stress response
5735	Ezrin	gi|744614044	67.571	6.79	186	44	Links actin to the plasma membrane
6004	Peroxiredoxin-5, mitochondrial	gi|47523086	17.484	5.71	126	42	Metabolic process
6108	Phosphoglycerate mutase 1	gi|4505753	28.9	6.67	222	62	Metabolic process
6310	Septin 2	gi|345090969	41.813	6.19	215	51	Cytokinesis
7733	Elongation factor 2	gi|335282386	96.262	6.41	351	47	Protein synthesis
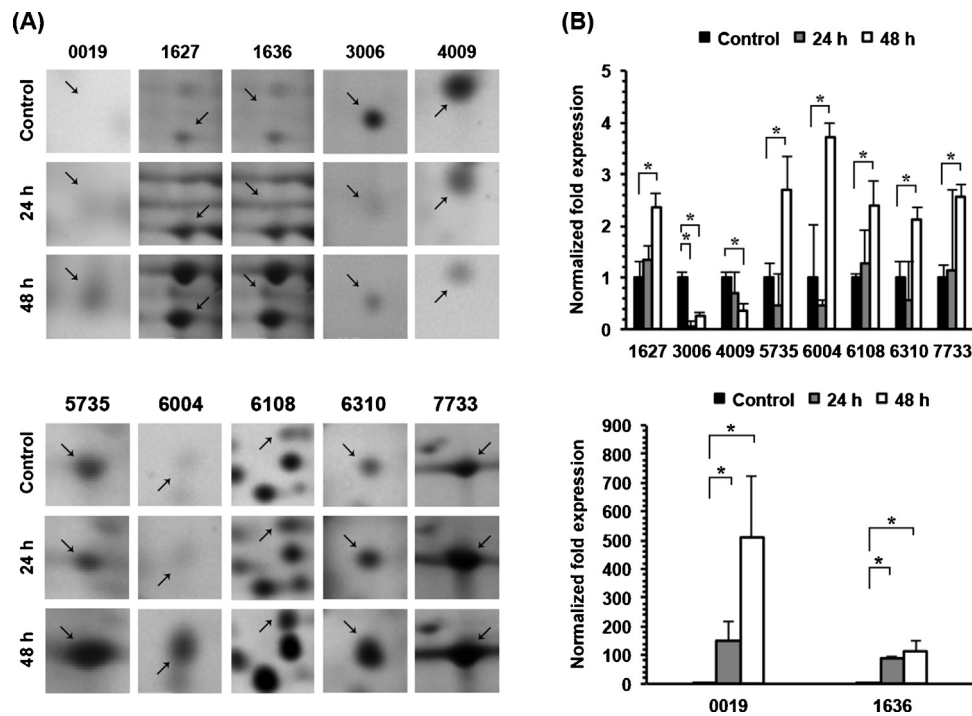
Fig. 4. Representative gel images showing spots that displayed significantly differential expression. (A) The magnified pictures represent the proteomic analysis of control PK-Neo (upper panel) and PK-PDCoV-N cells (middle and lower panels) and exhibited differentially regulated proteins identified in N gene-expressing cells. Four-digit numbers on the top represent individual spot identification. (B) The quantity of each spot was normalized based on the total valid spot intensity for each gel and the relative fold change of each spot was then calculated between control PK-Neo and PK-PDCoV-N cells. Data representing three independent 2DE experiments for each sample were statistically analyzed and error bars represent standard deviations. *$P = 0.001$–0.05.
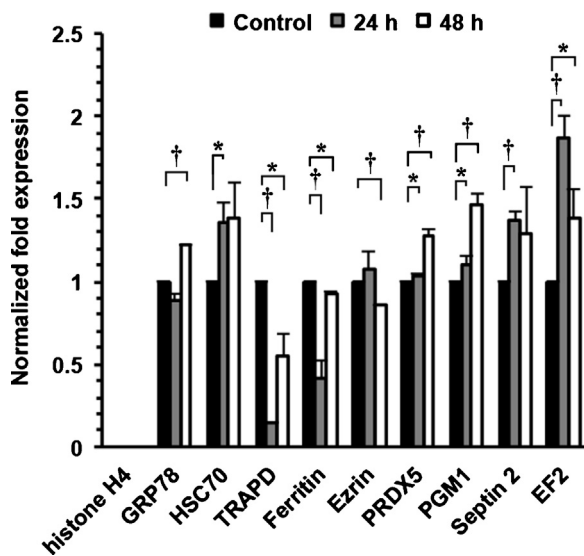
3.4. Altered expression of the heat shock protein 70 (HSP70) family in response to the PDCoV N protein

Two members of the HSP70 family, glucose-regulated protein 78 (GRP78) and heat shock cognate 70-kDa protein (HSC70), were found to be up-regulated in the PDCoV N-expressing cells by the proteomic analysis. To further verify the dynamic alterations in

Fig. 5. Transcriptional alteration of identified cellular genes in PK-PDCoV-N cells. The mRNA level of each gene was assessed by quantitative real-time RT-PCR and normalized to that of porcine β-actin. Relative quantities (RQ) of mRNA accumulation were evaluated by $2^{-\Delta\Delta Ct}$ method and the relative fold change of each gene was then calculated between control PK-Neo and PK-PDCoV-N cells. Results are expressed as the mean values from three independent experiments in duplicate and error bars represent standard deviations. *$P = 0.001$–0.05; †$P < 0.001$.

expression of these stress-response proteins under the influence of PDCoV N, we performed time-course Western blot analysis. Total cellular lysates were prepared from PK-PDCoV-N cells at different time points, and the expression kinetics of the GRP78 and HSC70 was compared between control and N protein-containing extracts. Higher expression of both proteins was first evident in PK-PDCoV-N cells as early as at 12 h post-seeding in comparison with control PK-Neo cells, and the production of both proteins was persistently high during the later time points, suggesting that their enhanced expression is dependent on the N protein (Fig. 6). These results were consistent with the proteomic analysis of 2DE gels and real-time RT-PCR, demonstrating that the synthesis of GRP78 and HSC70 is indeed up-regulated in response to expression of the N protein of PDCoV.
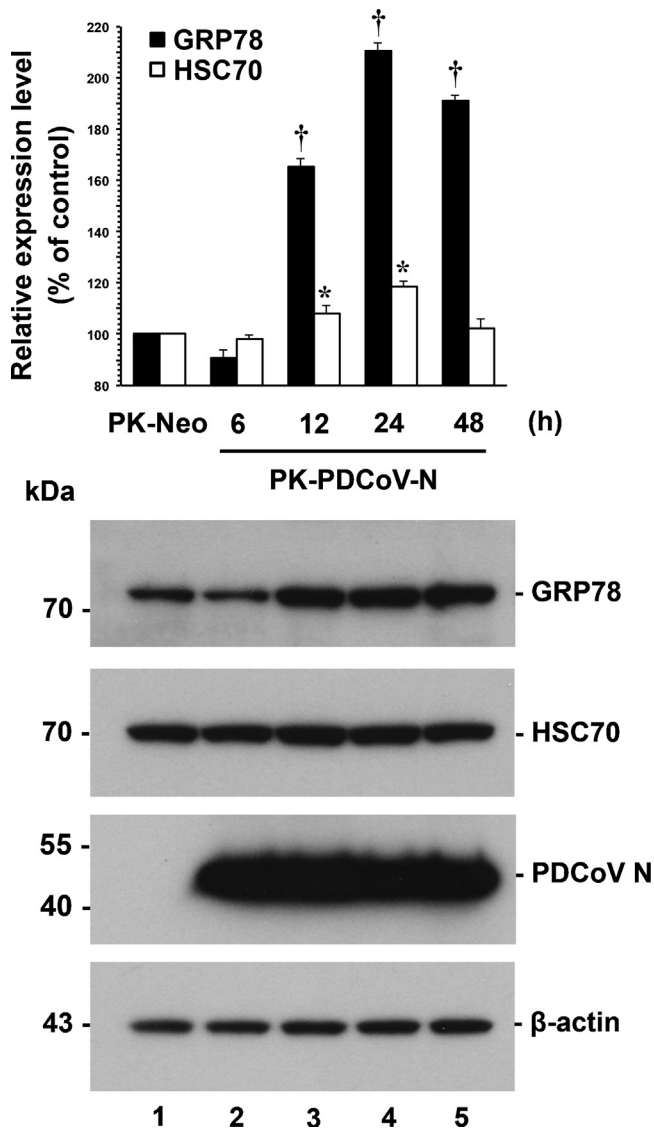
4. Discussion

Since viruses are obligate intracellular parasites, they must utilize the cellular machinery and biosynthetic components of the host cell for their own replication. After viral infection, the infected cells launch a number of host antiviral defensive responses, which are turned on to eliminate the invading viruses. On the other hand, viruses employ their own evasion strategies to complete their replication and to successfully spread to neighboring cells. This series of interactions between the virus and host results in compensatory modifications in cellular gene production. Accordingly, numerous studies have been extensively conducted by means of various molecular and genomic methods to understand how the altered host gene expression affects viral infection and the associated pathogenic processes. The proteomic analysis coupling high-resolution 2DE and MALDI-TOF/MS is a tool that can generate ample data on cellular protein profiles modified by viral replication. With the proteomic techniques, it is now possible to identify relative changes in protein abundance for evaluation of host cellular

Fig. 6. Differential expression of the HSP70 family in PK-PDCoV-N cells. Cell lysates were prepared from PDCoV N gene-expressing PK cells at indicated time points and immunoblotted to determine the expression profile of each protein with antibodies specific for GRP78 and HSC70 (top to second panels). The blot was also reacted with anti-His tag (third panel) and anti-β-actin (bottom panel) antibodies to confirm the status of N expression and equal protein loading, respectively. Each cellular protein expression was quantitatively analyzed by densitometry in terms of the relative density value to the β-actin gene and PK-PDCoV-N sample results were compared to PK-control results. Values are representative of the mean from three independent experiments and error bars denote standard deviations. $*P = 0.001–0.05$; $†P < 0.001$.

responses to viral infection or viral protein expression and to gain specific insights into the cellular mechanisms involved in viral pathogenesis (Alfonso et al., 2004; Brasier et al., 2004; Neuman et al., 2008; Oh and Lee, 2012; Ringrose et al., 2008; Sagong and Lee, 2010; Zhang et al., 2008). In the present work, a proteomic approach was applied for profiling the global protein expression changes in host cells in response to the N protein of PDCoV, which is a major constituent of the virion and infected cells. Therefore, we initially established a porcine cell line stably expressing the PDCoV N protein and then characterized the N protein produced in those cells. Due to the absence of cysteine residues, a disulfide-linked homodimeric N protein of PDCoV was not detected in PK-PDCoV-N cells. Rather, the PDCoV N protein was shown to be self-assembled via non-covalent oligomerization as a structural component for formation of the viral capsid. Interestingly, the N protein of PDCoV

was found to be predominantly present in both the cytoplasm and nucleolus of PK-PDCoV-N cells. The localization of nidovirus N proteins to the nucleolus may be necessary for control of RNA synthesis or ribosome biogenesis via association with ribosomal subunits and interaction with nucleolar proteins (Chen et al., 2002; Lee et al., 2006; Wurm et al., 2001; Yoo et al., 2003;). Similarly, the PDCoV N protein may participate in such a viral strategy to favor viral replication and pathogenesis. In addition, the nucleolar localization sequence detector program (http://www.compbio.dundee.ac.uk/www-nod/) predicted that PDCoV N harbors a putative nucleolar localization signal (NoLS) consisting of a stretch of basic amino acids. Therefore, further research is needed to identify a functional NoLS to confirm the intracellular localization of the PDCoV N protein. These biological characteristics of N gene-expressing cells have yet to be confirmed using an authentic N protein in PDCoV-infected cells, but according to our results, PDCoV N appears to act as a multifunctional protein playing structural and non-structural roles contributing to completion of viral replication. Our proteomic data revealed that 10 differentially expressed cellular proteins are identifiable in PDCoV N gene-expressing porcine cells. The proteins that we identified in this study are involved in diverse cellular processes: metabolism, the stress response, protein biosynthesis and transport, cytoskeleton networks and cell communication, and cell division. The significance of the functional roles of the selected host proteins affected by the interaction of the PDCoV N protein with the host cell is discussed below.

The most interesting finding in the present study is that two cellular chaperone proteins belonging to the HSP70 family are up-regulated concomitantly by the N protein of PDCoV. The first up-regulated protein is GRP78 in cells expressing the PDCoV N protein, which is associated with endoplasmic reticulum (ER) stress. In eukaryotic cells, the ER is the major site for synthesis and folding of transmembrane and secreted proteins, and accordingly, animal viruses also use the ER as a site of synthesis and processing of their own proteins. The amount of protein entering the ER can differ under physiological and environmental conditions. If protein synthesis exceeds the folding capacity of the ER, unfolded proteins accumulate there, resulting in ER stress. To maintain the ER homeostasis, cells have developed a signaling pathway known as the unfolded protein response (UPR) that transmits signals across the ER membrane to the cytosol and the nucleus and ultimately reduces protein translation and enhances the ER folding capacity by up-regulating chaperone proteins (Ron and Walter, 2007). Coronavirus infection of cultured cells is known to cause ER stress and to induce the UPR, which then crosstalks with various cellular signaling pathways, including mitogen-activated protein kinase cascades, autophagy, apoptosis, and innate immune responses, indicating the involvement of UPR activation in virus–host interactions and viral pathogenesis (Fung et al., 2014; Fung and Liu, 2014). More interestingly, global proteomic and microarray analyses have shown that the expression of chaperon proteins, such as GRP78 and GRP94, is up-regulated in cells infected with a human coronavirus or in cells expressing the S2 subunit (Jiang et al., 2005; Yeung et al., 2008). Furthermore, the N protein of PEDV, another porcine coronavirus, overexpression was shown to trigger ER stress (Xu et al., 2013). Thus, it appears that PDCoV infection may induce ER stress and the UPR, leading to the up-regulation of GRP78 to counteract the ER stress; hence, the N protein may be responsible for this stress response pathway. The second identified HSP70 family protein is HSC70, also known as heat shock 70-kDa protein 8 (HSPA8). HSC70 is a molecular chaperone with multiple functions in protein folding and trafficking in all eukaryotic cells and in protecting cells from apoptosis or a wide array of stressors such as heat and infection (Morano, 2007; Powers et al., 2008; Takayama et al., 1999). Accumulating evidence has shown that HSC70 plays important roles in certain processes involved in viral

infection by modulating cell entry, virion disassembly and assembly, and the cellular antiviral response and apoptosis (Chuang et al., 2015; Gutiérrez et al., 2010; Ivanovic et al., 2007; Liu et al., 2013; Radhakrishnan et al., 2010; Yan et al., 2010). Apoptosis is considered an innate defense mechanism that limits propagation of a virus by eliminating infected cells (Everett and McFadden, 1999). Therefore, many viruses have evolved to employ various strategies that inhibit apoptosis in order to prevent premature cell death, thereby securing sufficient time for progeny production. Thus, a conceivable explanation is that PDCoV may take the advantage of suppressing apoptosis by up-regulating HSC70 in the early phase of the infection, and the N protein seems to be involved in this mechanism. In addition, HSC70 mediates the nuclear export of the influenza virus ribonucleoprotein complex via interaction with viral proteins M1 and NS2 (Watanabe et al., 2006, 2014). In the present study, we found that PDCoV N can be localized to the nucleolus in N-expressing cells. On the other hand, N proteins must be trafficked from the nucleolus to the cytoplasm to accomplish nucleocapsid assembly as well as viral RNA synthesis and virus–host interactions. According to our results and existing data, HSC70 may facilitate the export of PDCoV N from the nucleolus to complete the viral life cycle.

Like many other viruses, coronaviruses turn off host protein translation, while continuing to the synthesis of their own gene products to finish viral replication. One of the mechanisms behind this translational suppression is through interaction of the N protein with elongation factor 1α (EF1α), a major translation factor in mammalian cells (Zhou et al., 2008). In the present study, the amount of another translational factor, EF2, was affected by the host response to the PDCoV N protein. Although we do not know whether the increased expression of EF2 is related to its binding to PDCoV N, such differential expression of a translation factor may be associated with regulation of both host and viral protein synthesis. We also found that expression of the cytoskeletal protein ezrin is significantly enhanced by the N protein. Ezrin is a member of the ezrin–moesin–radixin (EMR) family of host cytoskeletal proteins that organize the cortical cytoskeleton by mediating interactions between actin and the plasma membrane proteins and function as signal transducers in numerous signaling pathways (Neisch and Fehon, 2011). The EMR also modulate RNA virus infection by regulating stable and dynamic microtubule formation (Bukong et al., 2013; Haedicke et al., 2008; Naghavi et al., 2007). Given the biological features of the EMR proteins, the up-regulation of ezrin in our study suggests that the PDCoV N protein may manipulate the host cytoskeletal network and cell signaling, possibly to facilitate the processes of viral infection and replication.

In contrast, the expression of translocon-associated protein subunit delta (TRAPD) is suppressed in cells expressing the PDCoV N protein, according to our results. TRAPD is a part of the TRAP complex that is involved in translocating proteins across the ER membrane and in regulating the retention of ER resident proteins (Fons et al., 2003). Coronaviruses acquire their lipid envelop via budding of the nucleocapsid through the ER–Golgi intermediate compartment (McBride et al., 2014). The down-regulation of TRAPD may lead to the release of cellular proteins from the ER during PDCoV replication, which in turn, promotes translocation of envelope-associated viral structural proteins to the ER membrane – the site of budding – to facilitate virus assembly. Eukaryotic cells reprogram their metabolism to adapt to stress-induced damage in response to environmental stressors. Among our differentially expressed proteins, some are either directly or indirectly involved in metabolism. One hypothesis that can explain this result is that production of the N protein affects cellular biosynthesis by modulating the expression of metabolism-related proteins, which in turn remodels the intracellular environment for optimal PDCoV replication.

In conclusion, to our knowledge, this is the first report of a proteomic analysis of cellular responses to the PDCoV N protein. Although definite functions of the proteins that we identified here were not determined, it is likely that alterations in their expression are involved in virus–host interactions. To resolve these questions as well as performing various PDCoV research, obtaining a Korean PDCoV isolate that can grow in cell culture is necessary; we are currently working on this task. In future studies, we are planning to assess cellular responses to PDCoV by proteomic analysis to validate our present data; the proteins that are differentially expressed in the cells overexpressing PDCoV N or in the cells infected with PDCoV can be analyzed in detail in order to identify their precise function in the replication of PDCoV. On the other hand, one limitation of the proteomic methodology used in this study is the inability to reliably detect low-molecular-weight or low-abundance proteins such as cytokines, which are involved in the host immune response. Therefore, more comprehensive works are also needed to expand our present findings and to explore other proteins that may play a role in host responses to this protein. Nevertheless, the data presented here are expected to advance the knowledge about the molecular mechanisms associated with PDCoV–host interactions and viral pathogenesis.

Acknowledgment

References

Alfonso, P., Rivera, J., Hernáez, B., Alonso, C., Escribano, J.M., 2004. Identification of cellular proteins modified in response to African swine fever virus infection by proteomics. Proteomics 4, 2037–2046.

Bradford, M.M., 1976. A rapid and sensitive method for the quantitation of microgram quantities of protein utilizing the principle of protein–dye binding. Anal. Biochem. 72, 248–254.

Brasier, A.R., Spratt, H., Wu, Z., Boldogh, I., Zhang, Y., Garofalo, R.P., Casola, A., Pashmi, J., Haag, A., Luxon, B., Kurosky, A., 2004. Nuclear heat shock response and novel nuclear domain 10 reorganization in respiratory syncytial virus-infected a549 cells identified by high-resolution two-dimensional gel electrophoresis. J. Virol. 78, 11461–11476.

Bukong, T.N., Kodys, K., Szabo, G., 2013. Human ezrin–moesin–radixin proteins modulate hepatitis C virus infection. Hepatology 58, 1569–1579.

Chen, H., Wurm, T., Britton, P., Brooks, G., Hiscox, J.A., 2002. Interaction of the coronavirus nucleoprotein with nucleolar antigens and the host cell. J. Virol. 76, 5233–5250.

Chuang, C.K., Yang, T.H., Chen, T.H., Yang, C.F., Chen, W.J., 2015. Heat shock cognate protein 70 isoform D is required for clathrin-dependent endocytosis of Japanese encephalitis virus in C6/36 cells. J. Gen. Virol. 96, 793–803.

de Groot, R.J., Baker, S.C., Baric, R., Enjuanes, L., Gorbalenya, A.E., Holmes, K.V., Perlman, S., Poon, L., Rottier, P.J.M., Talbot, P.J., Woo, P.C.Y., Ziebuhr, J., 2011. Coronaviridae. In: King, A.M.Q., Adams, M.J., Carstens, E.B., Lefkowitz, E.J. (Eds.), Virus Taxonomy: Ninth Report of the International Committee on Taxonomy of Viruses. Elsevier, Oxford, pp. 806–828.

Everett, H., McFadden, G., 1999. Apoptosis: an innate immune response to virus infection. Trends Microbiol. 7, 160–165.

Fernandez, J., Gharahdaghi, F., Mische, S.M., 1998. Routine identification of proteins from sodium dodecyl sulfate-polyacrylamide gel electrophoresis (SDS-PAGE) gels or polyvinyl difluoride membranes using matrix assisted laser desorption/ionization-time of flight-mass spectrometry (MALDI-TOF-MS). Electrophoresis 19, 1036–1045.

Fons, R.D., Bogert, B.A., Hegde, R.S., 2003. Substrate-specific function of the translocon-associated protein complex during translocation across the ER membrane. J. Cell Biol. 160, 529–539.

Fung, T.S., Huang, M., Liu, D.X., 2014. Coronavirus-induced ER stress response and its involvement in regulation of coronavirus–host interactions. Virus Res. 194, 110–123.

Fung, T.S., Liu, D.X., 2014. Coronavirus infection, ER stress, apoptosis and innate immunity. Front. Microbiol. 5, 1–13.

Gutiérrez, M., Isa, P., Sánchez-San, Martin, C., Pérez-Vargas, J., Espinosa, R., Arias, C.F., López, S., 2010. Different rotavirus strains enter MA104 cells through different endocytic pathways: the role of clathrin-mediated endocytosis. J. Virol. 84, 9161–9169.

Gygi, S.P., Rochon, Y., Franza, B.R., Aebersold, R., 1999. Correlation between protein and mRNA abundance in yeast. Mol. Cell. Biol. 19, 1720–1730.

Haedicke, J., de Los Santos, K., Goff, S.P., Naghavi, M.H., 2008. The ezrin–radixin–moesin family member ezrin regulates stable microtubule formation and retroviral infection. J. Virol. 82, 4665–4670.

Hiscox, J.A., Wurm, T., Wilson, L., Britton, P., Cavanagh, D., Brooks, G., 2001. The coronavirus infectious bronchitis virus nucleoprotein localizes to the nucleolus. J. Virol. 75, 506–512.

Ivanovic, T., Agosto, M.A., Chandran, K., Nibert, M.L., 2007. A role for molecular chaperone Hsc70 in reovirus outer capsid disassembly. J. Biol. Chem. 282, 12210–12219.

Jiang, X.S., Tang, L.Y., Dai, J., Zhou, H., Li, S.J., Xia, Q.C., Wu, J.R., Zeng, R., 2005. Quantitative analysis of severe acute respiratory syndrome (SARS)-associated coronavirus-infected cells using proteomic approaches: implications for cellular responses to virus infection. Mol. Cell Proteomics 4, 902–913.

Jung, K., Hu, H., Eyerly, B., Lu, Z., Chepngeno, J., Saif, L.J., 2015. Pathogenicity of 2 porcine deltacoronavirus strains in gnotobiotic pigs. Emerg. Infect. Dis. 21, 650–654.

Kim, Y., Lee, C., 2013. Ribavirin efficiently suppresses porcine nidovirus replication. Virus Res. 171, 44–53.

Lai, M.C., Perlman, S., Anderson, L.J., 2007. Coronaviridae. In: Knipe, D.M., Howley, P.M., Griffin, D.E., Martin, M.A., Lamb, R.A., Roizman, B., Straus, S.E. (Eds.), Fields Virology. , fifth ed. Lippincott Williams & Wilkins, Philadelphia, PA, pp. 1305–1336.

Lee, C., Hodgins, D.C., Calvert, J.G., Welch, S.K., Jolie, R., Yoo, D., 2006. The nuclear localization signal of the PRRS virus nucleocapsid protein viral replication in vitro and antibody response in vivo. Adv. Exp. Med. Biol. 581, 145–148.

Lee, S., Lee, C., 2014. Complete genome characterization of Korean porcine deltacoronavirus strain KOR/KNU14-04/2014. Genome Announc. 2, e01191–e1214.

Lee, C., Yoo, D., 2006. The small envelope protein of porcine reproductive and respiratory syndrome virus possesses ion channel protein-like properties. Virology 355, 30–43.

Lee, Y.J., Park, C.K., Nam, E., Kim, S.H., Lee, O.S., Lee, D.S., Lee, C., 2010. Generation of a porcine alveolar macrophage cell line for the growth of porcine reproductive and respiratory syndrome virus. J. Virol. Methods 163, 410–415.

Li, G., Chen, Q., Harmon, K.M., Yoon, K.J., Schwartz, K.J., Hoogland, M.J., Gauger, P.C., Main, R.G., Zhang, J., 2014. Full-length genome sequence of porcine deltacoronavirus strain USA/IA/2014/8734. Genome Announc. 2, e00278–e314.

Livak, K.J., Schmittgen, T.D., 2001. Analysis of relative gene expression data using real-time quantitative PCR and the 2(−Delta Delta C(T)) method. Methods 25, 402–408.

Liu, Z., Wu, S.W., Lei, C.Q., Zhou, Q., Li, S., Shu, H.B., Wang, Y.Y., 2013. Heat shock cognate 71 (HSC71) regulates cellular antiviral response by impairing formation of VISA aggregates. Protein Cell 4, 373–382.

Marthaler, D., Jiang, Y., Collins, J., Rossow, K., 2014a. Complete genome sequence of strain SDCV/USA/Illinois121/2014, a porcine deltacoronavirus from the United States. Genome Announc. 2, e00218–e314.

Marthaler, D., Raymond, L., Jiang, Y., Collins, J., Rossow, K., Rovira, A., 2014b. Rapid detection, complete genome sequencing, and phylogenetic analysis of porcine deltacoronavirus. Emerg. Infect. Dis. 20, 1347–1350.

McBride, R., van Zyl, M., Fielding, B.C., 2014. The coronavirus nucleocapsid is a multifunctional protein. Viruses 6, 2991–3018.

Morano, K.A., 2007. New tricks for an old dog: the evolving world of Hsp70. Ann. N. Y. Acad. Sci. 1113, 1–14.

Naghavi, M.H., Valente, S., Hatziioannou, T., de Los Santos, K., Wen, Y., Mott, C., Gundersen, G.G., Goff, S.P., 2007. Moesin regulates stable microtubule formation and limits retroviral infection in cultured cells. EMBO 26, 41–52.

Nam, E., Lee, C., 2010. Contribution of the porcine aminopeptidase N (CD13) receptor density to porcine epidemic diarrhea virus infection. Vet. Microbiol. 144, 41–50.

Neisch, A.L., Fehon, R.G., 2011. Ezrin, radixin and moesin: key regulators of membrane–cortex interactions and signaling. Curr. Opin. Cell Biol. 23, 377–382.

Neuman, B.W., Joseph, J.S., Saikatendu, K.S., Serrano, P., Chatterjee, A., Johnson, M.A., Liao, L., Klaus, J.P., Yates III, J.R., Wüthrich, K., Stevens, R.C., Buchmeier, M.J., Kuhn, P., 2008. Proteomics analysis unravels the functional repertoire of coronavirus nonstructural protein 3. J. Virol. 82, 5279–5294.

Oakley, B.R., Kirsch, D.R., Morris, N.R., 1980. A simplified ultrasensitive silver stain for detecting proteins in polyacrylamide gels. Anal. Biochem. 105, 361–363.

Oh, J., Lee, C., 2012. Proteomic characterization of a novel structural protein ORF5a of porcine reproductive and respiratory syndrome virus. Virus Res. 169, 255–263.

Powers, M.V., Clarke, P.A., Workman, P., 2008. Dual targeting of HSC70 and HSP72 inhibits HSP90 function and induces tumor-specific apoptosis. Cancer Cell 14, 250–262.

Radhakrishnan, A., Yeo, D., Brown, G., Myaing, M.Z., Iyer, L.R., Fleck, R., Tan, B.H., Aitken, J., Sanmun, D., Tang, K., Yarwood, A., Brink, J., Sugrue, R.J., 2010. Protein analysis of purified respiratory syncytial virus particles reveals an important role for heat shock protein 90 in virus particle assembly. Mol. Cell Proteomics 9, 1829–1848.

Ringrose, J.H., Jeeninga, R.E., Berkhout, B., Speijer, D., 2008. Proteomic studies reveal coordinated changes in T-cell expression patterns upon infection with human immunodeficiency virus type 1. J. Virol. 82, 4320–4330.

Ron, D., Walter, P., 2007. Signal integration in the endoplasmic reticulum unfolded protein response. Nat. Rev. Mol. Cell Biol. 8, 519–529.

Sagong, M., Lee, C., 2010. Differential cellular expression in continuous porcine alveolar macrophages regulated by the porcine reproductive and respiratory syndrome virus nucleocapsid protein. Virus Res. 151, 88–96.

Sagong, M., Lee, C., 2011. Porcine reproductive and respiratory syndrome virus nucleocapsid protein modulates interferon-β production by inhibiting IRF3 activation in immortalized porcine alveolar macrophages. Arch. Virol. 156, 2187–2195.

Sambrook, J., Russell, D.W., 2001. Molecular Cloning: A Laboratory Manual, third ed. Cold Spring Harbor Laboratory Press, Cold Spring Harbor, NY.

Shevchenko, A., Wilm, M., Vorm, O., Mann, M., 1996. Mass spectrometric sequencing of proteins silver-stained polyacrylamide gels. Anal. Chem. 68, 850–858.

Takayama, S., Xie, Z., Reed, J.C., 1999. An evolutionarily conserved family of Hsp70/Hsc70 molecular chaperone regulators. J. Biol. Chem. 274, 781–786.

Wang, L., Byrum, B., Zhang, Y., 2014. Detection and genetic characterization of deltacoronavirus in pigs, Ohio, USA, 2014. Emerg. Infect. Dis. 20, 1227–1230.

Watanabe, K., Fuse, T., Asano, I., Tsukahara, F., Maru, Y., Nagata, K., Kitazato, K., Kobayashi, N., 2006. Identification of Hsc70 as an influenza virus matrix protein (M1) binding factor involved in the virus life cycle. FEBS Lett. 580, 5785–5790.

Watanabe, K., Shimizu, T., Noda, S., Tsukahara, F., Maru, Y., Kobayashi, N., 2014. Nuclear export of the influenza virus ribonucleoprotein complex: interaction of Hsc70 with viral proteins M1 and NS2. FEBS Open Bio 4, 683–688.

Woo, P.C., Lau, S.K., Lam, C.S., Lau, C.C., Tsang, A.K., Lau, J.H., Bai, R., Teng, J.L., Tsang, C.C., Wang, M., Zheng, B.J., Chan, K.H., Yuen, K.Y., 2012. Discovery of seven novel mammalian and avian coronaviruses in the genus deltacoronavirus supports bat coronaviruses as the gene source of alphacoronavirus and betacoronavirus and avian coronaviruses as the gene source of gammacoronavirus and deltacoronavirus. J. Virol. 86, 3995–4008.

Wootton, S.K., Yoo, D., 2003. Homo-oligomerization of the porcine reproductive and respiratory syndrome virus nucleocapsid protein and the role of disulfide linkages. J. Virol. 77, 4546–4557.

Wurm, T., Chen, H., Hodgson, T., Britton, P., Brooks, G., Hiscox, J.A., 2001. Localization to the nucleolus is a common feature of coronavirus nucleoproteins, and the protein may disrupt host cell division. J. Virol. 75, 9345–9356.

Xu, X., Zhang, H., Zhang, Q., Huang, Y., Dong, J., Liang, Y., Liu, H.-J., Tong, D., 2013. Porcine epidemic diarrhea N protein prolongs S-phase cell cycle, induces endoplasmic reticulum stress, and up-regulates interleukin-8 expression. Vet. Microbiol. 164, 212–221.

Yan, F., Xia, D., Hu, J., Yuan, H., Zou, T., Zhou, Q., Liang, L., Qi, Y., Xu, H., 2010. Heat shock cognate protein 70 gene is required for prevention of apoptosis induced by WSSV infection. Arch. Virol. 155, 1077–1083.

Yeung, B.H., Kwan, B.W., He, Q.Y., Lee, A.S., Liu, J., Wong, A.S., 2008. Glucose-regulated protein 78 as a novel effector of BRCA1 for inhibiting stress-induced apoptosis. Oncogene 27, 6782–6789.

Yoo, D., Wootton, S.K., Li, G., Song, C., Rowland, R.R., 2003. Colocalization and interaction of the porcine arterivirus nucleocapsid protein with the small nucleolar RNA-associated protein fibrillarin. J. Virol. 77, 12173–12183.

Zhang, J., Li, D., Zheng, Y., Cui, Y., Feng, K., Zhou, J., Wu, J., 2008. Proteomic profiling of hepatitis B virus-related hepatocellular carcinoma in China: a SELDI-TOF-MS study. Int. J. Clin. Exp. Pathol. 1, 352–361.

Zhang, H., Guo, X., Ge, X., Chen, Y., Sun, Q., Yang, H., 2009. Changes in the cellular proteins of pulmonary alveolar macrophage infected with porcine reproductive and respiratory syndrome virus by proteomics analysis. J. Proteome Res. 8, 3091–3097.

Zhou, B., Liu, J., Wang, Q., Liu, X., Li, X., Li, P., Ma, Q., Cao, C., 2008. The nucleocapsid protein of severe acute respiratory syndrome coronavirus inhibits cell cytokinesis and proliferation by interacting with translation elongation factor 1alpha. J. Virol. 82, 6962–6971.